Journal of Sound and Vibration (2000) **229**(3), 709–735
doi:10.1006/jsvi.1999.2512, available online at http://www.idealibrary.com on IDEAL®

CURVE SQUEAL OF TRAIN WHEELS, PART 3: ACTIVE CONTROL

MARIA A. HECKL

Department of Mathematics, Keele University, Keele, Staffordshire ST5 5BG, England

AND

X. Y. HUANG

School of Mechanical and Production Engineering, Nanyang Technological University, Nanyang Avenue, Singapore 639798, *Singapore*

(*Received* 25 *August* 1998, *and in final form* 5 *August* 1999)

This paper presents a new method to annul the squeal noise that is produced by trains traversing a curve. The method is a special form of active control, applied to suppress the bending oscillations of a squealing wheel. It is essentially a feedback system with the following components: sensor, narrowband filter, phase-shifter, amplifier and actuator. The control signal driving the actuator has only a single frequency (set at the filter), and that frequency typically corresponds to one of the bending modes of the wheel. Two versions of the feedback system are considered. In the first version, the actuator exerts a control force on the wheel, and in the second version, the actuator imposes a velocity on the rail. A mathematical model is presented and predictions are made for the performance of both versions. The coupling of the different wheel modes by the control system is discussed. A model rig is described which was used for a practical demonstration of this form of active control. Differences from more conventional forms of active control are pointed out.

1. INTRODUCTION

Curve squeal is one of the most disturbing types of noise from rail-based public transport systems. The frequency spectrum of curve squeal is dominated by a few (between 1 and 4) very sharp peaks. It is the frequency of the peaks (typically between 1500 and 5000 Hz, where the human ear is very sensitive) and the height of the peaks (more than 20 dB(A) above the rolling noise) which make curve squeal such an unpleasant experience [1]. The need to control curve squeal is evident.

Cure squeal is generated if a train traversing a bend performs a crabbing motion with its wheels because they cannot align themselves tangentially to the rail. As a consequence of this crabbing motion, a dry friction force acts on the wheels in the lateral direction, this excites bending oscillations of the wheels, and they radiate sound into the surrounding air [2–4].

0022-460X/00/030709 + 27 $35.00/0

The dry friction force has a stick/slip behaviour and depends on the difference between wheel and rail velocity. There is thus a feedback between the wheel oscillation and the friction force driving this oscillation. This leads to some bending modes becoming "self-excited" at their resonance frequencies, and these are found as peaks in the frequency spectrum of curve squeal. The slip behaviour and the stick behaviour of the friction force play two different roles. The slip behaviour is responsible for the instability of some wheel modes and drives them to grow exponentially. This occurs at low-velocity amplitudes. The stick behaviour is responsible for the limitation of this growth and imposes a limit cycle with a finite velocity amplitude. This occurs at velocity amplitudes that are high enough to be close to the crabbing speed [5].

Many measures to reduce curve squeal have been put into practice. Remington's article [4] contains a comprehensive overview. Wheel-related measures include application of damping [1, 2, 4, 6–8], design of acoustically optimized wheels [6–8], use of resilient wheels [3, 8], and use of trucks with some form of self-steering [1, 3, 4, 8]. Rail-related measures include widening of squeal-prone curves [3, 4]. Measures that involve the wheel/rail contact include lubrication of curved sections of rail [1, 3, 4] and the use of friction modifiers, which change the friction characteristic in such a way that its instability-inducing tendency is countered [4].

The aim of this paper is to introduce and examine an alternative method of controlling squeal. It involves a special form of active control, which suppresses the instability of the wheel oscillation caused by the friction force. This form of active control is not entirely new. It has been successfully applied to other instabilities, such as the heat-driven noise of a Rijke tube [9], aerofoil flutter [10] and compressor surge [11]. Its application to a simple friction-driven system (a mass-spring oscillator with a single mode) has been studied theoretically by Heckl and Abrahams [12]. The active control of a friction-driven wheel, oscillating with several potentially unstable modes, is the topic of this paper.

Our form of active control differs from more conventional forms, in particular anti-vibration techniques, by a few crucial points. Conventional techniques work by superposition of a secondary vibration on a primary one in such a way that the combined vibration is weaker than the primary one. Our method works by interfering with the generation mechanism of the squeal: curve squeal is due to unstable bending oscillations of a train wheel, and we use active control to stabilize these oscillations. In contrast to our method, conventional techniques have high energy requirements throughout their operation and their effectiveness is very sensitive to errors in phase-shift and amplification.

Two versions of our active control system will be studied. The first version (the "wheel version") acts on the wheel and is shown in Figure 1(a); the second version (the "rail version") acts on the rail and is shown in Figure 1(b). The wheel version has the following components. A sensor (a structure-borne sound transducer that senses the velocity of the wheel, or alternatively a microphone that senses the noise radiated from the wheel) picks up a signal that is a measure of the wheel motion. This signal is passed through a narrowband filter, so that the filter-output signal has only a single frequency. This single-frequency signal is then phase-shifted and amplified. The resulting control signal is fed to a transducer attached to the wheel,

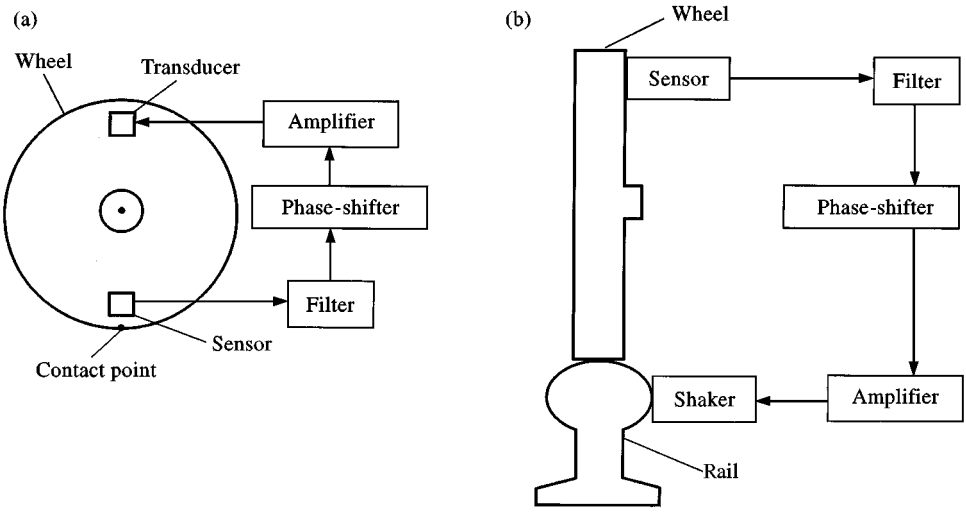

Figure 1. The active contol system: (a) control acting on the wheel; (b) control acting on the rail.

and this exerts a control force that excites bending oscillations of the wheel. The filter frequency, phase-shift and amplification are set at the instruments and remain constant throughout. The filter frequency is chosen to be identical with the squealing frequency (or one of the squealing frequencies if there are several peaks in the frequency spectrum of the squeal noise).

The rail version of the active control system differs from the wheel version only in the way the control signal is applied. Here, the control signal is fed into a shaker attached to the rail, which is assumed to have zero velocity if control were absent. This version of the control changes the difference between wheel and rail velocity and hence changes the behaviour of the friction force. In contrast, the wheel version of the control applies an extra force to the wheel in addition to the friction force.

A general description of the mathematical model for curve squeal and its control is given in Section 2. Two approaches are used to solve the integral equation that is the governing equation of the model. An iteration scheme for the time history of the wheel velocity is shown in Section 3. The complex eigenfrequencies of the wheel are calculated in Section 4. These three sections are based on the mathematical model, described in two companion papers [5, 13], which is extended to simulate the two versions of the active control system. A simple energy analysis, yielding analytical results for the stability behaviour, is shown in Section 5. In Section 6, numerical results for the time history and the complex eigenfrequencies are presented. A model rig has been constructed to simulate curve squeal, and to verify experimentally the active control system; this is described in Section 7.

2. GENERAL FORMULATION OF THE MATHEMATICAL MODEL

The motion of a friction-driven wheel has been studied in detail by Heckl and Abrahams [5]. They derived the following governing equation for the wheel

velocity v_w (see equation (2.3) in that paper, using notation F instead of F_f for the friction force, and v instead of v_w for the wheel velocity),

$$v_w(r, \varphi, t) = \int_{t'=0}^{t} F_f[v_w(r_f, \varphi_f, t')]\dot{G}(r, \varphi; r_f, \varphi_f; t - t')\,\mathrm{d}t'. \tag{2.1}$$

(r, φ) is an observer point on the wheel and (r_f, φ_f) is the contact point with the rail where the friction force acts. F_f is the friction force; it is dependent on the wheel velocity at the contact point, and this dependence is called the friction characteristic. G is the Green's function (displacement response) of the free wheel. The dot indicates partial differentiation with respect to time t. The Green's function is a superposition of bending modes of the wheel,

$$G(r, \varphi; r_f, \varphi_f; t - t') = \begin{cases} \text{real} \displaystyle\sum_{m=0}^{\infty} \sum_{n=1}^{\infty} g_{mn}(r, \varphi; r_f, \varphi_f)\mathrm{e}^{-\mathrm{i}(\omega_{mn} + \mathrm{i}\delta_{mn})(t-t')} & \text{for } t \geqslant t', \quad (2.2a) \\ 0 & \text{for } t < t'. \quad (2.2b) \end{cases}$$

ω_{mn}, δ_{mn} and g_{mn} are respectively the allowed frequency, growth rate and amplitude corresponding to mode (m, n) of the free wheel. These quantities can be measured for any wheel, or calculated theoretically for some simple wheel geometries.

Equation (2.1) needs to be extended to give a governing equation which models the active control of the friction-driven wheel.

2.1. WHEEL VERSION OF THE ACTIVE CONTROL SYSTEM

We consider the friction-driven wheel with the control system shown in Figure 1(a). The control force F_c exerted by the transducer is modelled as a point force (acting at point (r_c, φ_c)), which acts in addition to the friction force (at point (r_f, φ_f)) on the wheel. The motion of the wheel is then given by

$$v_w(r, \varphi, t) = \int_{t'=0}^{t} \{F_f[v_w(r_f, \varphi_f, t')]\dot{G}(r, \varphi; r_f, \varphi_f; t - t') + F_c(t')\dot{G}(r, \varphi; r_c, \varphi_c; t - t')\}\,\mathrm{d}t'. \tag{2.3}$$

This is an extension of equation (2.1), in that the wheel response to the friction force has been supplemented by that to the control force. In order to solve equation (2.3), $F_c(t')$ needs to be specified.

The sensor picks up the wheel velocity at some point, say (r_f, φ_f) (or some measure of this velocity), which consists of a superposition of different modes,

$$v_w(r_f, \varphi_f, t') = \text{real} \sum_{m=0}^{\infty} \sum_{n=1}^{\infty} A_{mn}(t')\mathrm{e}^{-\mathrm{i}\Omega_{mn}t'}, \tag{2.4}$$

with complex amplitudes A_{mn} and frequencies Ω_{mn}. The signal is passed through a narrowband filter tuned to one of the squeal frequencies, say Ω_{MN}. This frequency remains constant and is assumed to be equal to the eigenfrequency ω_{MN} of the free wheel. The filter output signal is real $[A_{MN}(t')\mathrm{e}^{-\mathrm{i}\Omega_{MN}t'}]$; this signal is phase-shifted by an amount ϕ and amplified by a factor α, generating a control signal which represents the control force

$$F_c(t') = \alpha \text{ real}[A_{MN}(t')\mathrm{e}^{-\mathrm{i}(\omega_{MN}t'+\phi)}]. \tag{2.5}$$

The amplification α and phase-shift ϕ are those of the entire feedback loop, including the sensor, filter, phase-shifter, amplifier and actuator. α is a ratio of force to velocity; it can be varied at the amplifier, but differs from the setting at the amplifier by an unknown (but constant) factor. The phase-shift ϕ can be varied at the phase-shifter; ϕ differs from the phase-shifter setting by an unknown additive constant.

The amplitude of the filter output signal, $A_{MN}(t')$, changes while the control is acting: it decreases continuously if the control works successfully, but it remains constant or even increases if the control system fails. The calculation of $A_{MN}(t')$ is shown in Section 2.3.

2.2. RAIL VERSION OF THE ACTIVE CONTROL SYSTEM

This version of the control is shown in Figure 1(b). The shaker changes the velocity difference at the contact point by the rail velocity v_r, and this affects the friction force. The governing equation is

$$v_w(r, \varphi, t) = \int_{t'=0}^{t} F_f[v_w(r_f, \varphi_f, t') - v_r(t')]\dot{G}(r, \varphi; r_f, \varphi_f; t - t')\,\mathrm{d}t'. \tag{2.6}$$

This is an extension of equation (2.1), in that the argument of the friction force has been supplemented by the rail velocity $v_r(t')$. In order to solve equation (2.6), $v_r(t')$ needs to be specified.

As for the wheel version of the active control, the control signal is a phase-shifted and amplified version of mode (M, N), which passes through the filter. This control signal represents the rail velocity.

$$v_r(t') = \alpha \text{ real}[A_{MN}(t')\mathrm{e}^{-\mathrm{i}(\omega_{MN}t'+\phi)}]. \tag{2.7}$$

Here, the amplification α is the ratio between two velocities.

2.3. CALCULATION OF THE CONTROL SIGNAL AMPLITUDE

$A_{MN}(t')$ is the complex amplitude of the filter output signal. It varies slowly within one period of the oscillation. $A_{MN}(t')$ is calculated as follows. Mode (M, N) is

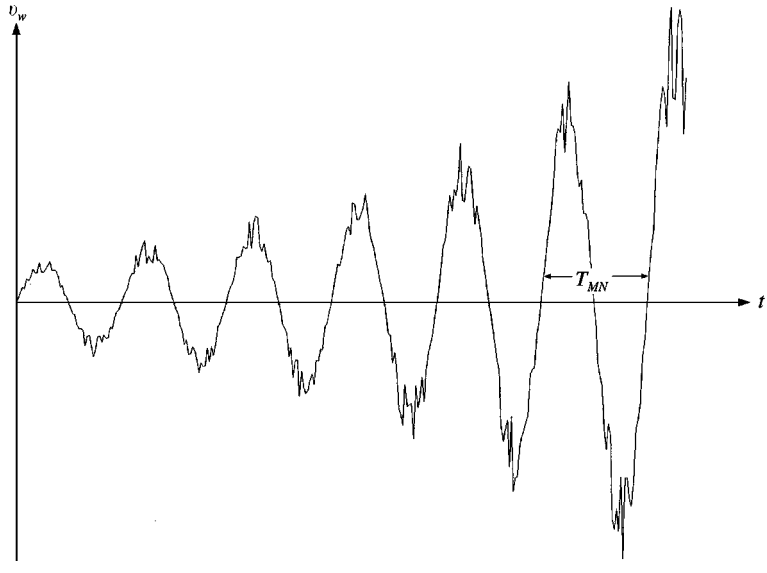

Figure 2. Time history of the wheel velocity.

assumed to be the dominant mode of the time history of the wheel velocity $v_w(r_f, \varphi_f, t)$ (see Figure 2). This time history can then be approximated by a Fourier series based on period $T_{MN} = 2\pi/\omega_{MN}$, with complex Fourier coefficients $c_0, c_1, c_2, \ldots$,

$$v_w(r_f, \varphi_f, t) \approx c_0 + \text{real} \sum_{k=-\infty}^{\infty} 2c_k e^{-i(2\pi k/T_{MN})t}. \tag{2.8}$$

The Fourier coefficient for $k = 1$ is taken to be the required A_{MN},

$$A_{MN}(t') = \frac{2}{T_{MN}} \int_{t'-T_{MN}}^{t'} v_w(r_f, \varphi_f, t) e^{i(2\pi/T_{MN})t} \, dt. \tag{2.9}$$

$A_{MN}(t')$ from equation (2.9) represents a good estimate for the amplitude of mode (M, N) if this mode dominates over all the other modes; this is the case if (M, N) is the only squealing mode. Otherwise, the result from equation (2.9) is also influenced by other dominant modes, and a coupling between these modes arises. This coupling is a feature of our control system, which can be tuned to only one frequency.

3. ITERATION FOR THE TIME HISTORY OF THE WHEEL VELOCITY

This section develops a method to calculate the time history of the wheel motion. It discretizes the time integrals for the wheel velocity to give an iteration moving forward in time. The considerations are based on those in section 4 of reference [5].

3.1. WHEEL VERSION OF THE ACTIVE CONTROL SYSTEM

We start with the integral equation (2.3) and insert the time derivative of the Green's function, using equation (2.2a) and the abbreviation

$$\psi_{mn} = \omega_{mn} + \mathrm{i}\delta_{mn}, \tag{3.1}$$

for its complex eigenfrequencies. The integral equation is then discretized with small time steps Δt. It is assumed that both forces, the friction force and the control force, are constant within each time step and can be approximated by the value from the previous time step. The remaining integrals can be calculated analytically, and the following iteration scheme for the time history of the wheel velocity (at point (r_f, φ_f)) is obtained:

$$v_w(t) = \text{real} \sum_{m=0}^{\infty} \sum_{n=1}^{\infty} (-\mathrm{i})\psi_{mn} \mathrm{e}^{-\mathrm{i}\psi_{mn}t} [g_{mn}(r_f, \varphi_f; r_f, \varphi_f) I_{mn}^{(f)}(t)$$

$$+ g_{mn}(r_f, \varphi_f; r_c, \varphi_c) I_{mn}^{(c)}(t)], \tag{3.2}$$

with

$$I_{mn}^{(f)}(t) = I_{mn}^{(f)}(t - \Delta t) + F_f(t - \Delta t) \frac{\mathrm{e}^{\mathrm{i}\psi_{mn}t}}{\mathrm{i}\psi_{mn}} (1 - \mathrm{e}^{-\mathrm{i}\psi_{mn}\Delta t}), \tag{3.3a}$$

$$I_{mn}^{(c)}(t) = I_{mn}^{(c)}(t - \Delta t) + F_c(t - \Delta t) \frac{\mathrm{e}^{\mathrm{i}\psi_{mn}t}}{\mathrm{i}\psi_{mn}} (1 - \mathrm{e}^{-\mathrm{i}\psi_{mn}\Delta t}). \tag{3.3b}$$

The friction force required in equation (3.3a) can be calculated from the friction characteristic $F_f(v_w)$ and the v_w-value from the previous time step. The control force required in equation (3.3b) is given by equation (2.5), where the control signal amplitude is calculated by discretizing the integral in equation (2.9), also with the time step Δt,

$$A_{MN}(t - \Delta t) = \frac{2\Delta t}{T_{MN}} \sum_{k=0}^{(T_{MN}/\Delta t)-1} v_w(t - T_{MN} + k\Delta t) \mathrm{e}^{\mathrm{i}(2\pi/T_{MN})(t + k\Delta t)}. \tag{3.4}$$

This requires the v_w-values of all time steps within the previous period.

The iteration starts at $t = 0$, and the following initial conditions are assumed:

$$v_w = 0 \quad \text{at } t = 0, \tag{3.5a}$$

$$F_c = 0 \quad \text{at } t = 0, \Delta t, 2\Delta t, \ldots, T_{MN} \quad \text{(no control during the initial period)}. \tag{3.5b}$$

3.2. RAIL VERSION OF THE ACTIVE CONTROL SYSTEM

Here, the considerations start with the integral equation (2.6). The manipulations of this integral equation are the same as in section 3.1 and lead to the following iteration scheme,

$$v_w(t) = \text{real} \sum_{m=0}^{\infty} \sum_{n=1}^{\infty} (-\mathrm{i})\psi_{mn} \mathrm{e}^{-\mathrm{i}\psi_{mn}t} g_{mn}(r_f, \varphi_f; r_f, \varphi_f) I_{mn}^{(f)}, \tag{3.6}$$

with

$$I_{mn}^{(f)}(t) = I_{mn}^{(f)}(t - \Delta t) + F_f[v_w(t - \Delta t) - v_r(t - \Delta t)] \frac{\mathrm{e}^{\mathrm{i}\psi_{mn}t}}{\mathrm{i}\psi_{mn}} (1 - \mathrm{e}^{-\mathrm{i}\psi_{mn}\Delta t}). \tag{3.7}$$

The friction force required in this equation can be calculated from the friction characteristic (now with an extra term in the argument), the v_w-value from the previous time step and the rail velocity given by equation (2.7). The control signal amplitude is calculated in the same way as in the previous section, to yield equation (3.4). The following initial conditions apply,

$$v_w = 0 \quad \text{at } t = 0, \text{ (iteration starts with zero velocity)}, \tag{3.8a}$$

$$v_r = 0 \quad \text{at } t = 0, \Delta t, 2\Delta t, \ldots, T_{MN} \quad \text{(no control during the initial period)}. \tag{3.8b}$$

4. COMPLEX EIGENFREQUENCIES OF THE CONTROLLED FRICTION-DRIVEN WHEEL

In contrast to the considerations in Section 3, which allowed any friction characteristic, we restrict our considerations in this section to linear friction characteristics. Here the friction force is assumed to have a mean part F_0 and an oscillatory part that depends linearly (factor γ) on the velocity difference at the wheel/rail contact point. The use of a linear friction force is valid at small oscillation amplitudes where the velocity difference does not reach the crabbing speed, i.e., where the friction force exhibits only slip behaviour, but no stick behaviour. The integral equations (2.3) and (2.6) for the wheel motion are then linear, and they can be used as a basis to calculate the eigenfrequencies Ψ_{mn} of the controlled friction-driven wheel. The derivation of the equations for the Ψ_{mn} is described in reference [13] for a friction-driven wheel without any form of control. The method is outlined for both versions of the active control system in Appendix A. Only a finite number of modes is considered ($m = 0, \ldots \mu$, $n = 1, \ldots, \nu$). The Ψ_{mn} are generally complex and composed of the real frequency Ω_{mn} and the growth rate Δ_{mn},

$$\Psi_{mn} = \Omega_{mn} + \mathrm{i}\Delta_{mn}. \tag{4.1}$$

The sign of Δ_{mn} indicates the stability behaviour of mode (m, n): if $\Delta_{mn} > 0$, the mode is unstable, and if $\Delta_{mn} \leqslant 0$, the mode is stable.

4.1. WHEEL VERSION OF THE ACTIVE CONTROL SYSTEM

The friction force is assumed to depend linearly on the difference between wheel velocity v_w and rail velocity v_r. Since v_r is zero for this version of the control system, the friction characteristic

$$F_f = F_0 + \gamma v_w \tag{4.2}$$

is used. If this is substituted into equation (2.3), a linear integral equation for v_w is obtained. The complex eigenfrequencies Ψ_{mn} are found to satisfy the following set of non-linear algebraic equations (see Appendix A),

$$\Psi_{mn}\frac{1}{2}\gamma\sum_{m'=0}^{\mu}\sum_{n'=1}^{\nu}\left[\frac{g_{m'n'}(r_f,\varphi_f;r_f,\varphi_f)}{\Psi_{mn}-\psi_{m'n'}}+\frac{g^*_{m'n'}(r_f,\varphi_f;r_f,\varphi_f)}{\Psi_{mn}+\psi^*_{m'n'}}\right]$$

$$+\frac{\alpha}{T_{MN}}C(\Psi_{mn})\frac{1}{2}\sum_{m'=0}^{\mu}\sum_{n'=1}^{\nu}\left[\frac{g_{m'n'}(r_f,\varphi_f;r_c,\varphi_c)}{\Psi_{mn}-\psi_{m'n'}}+\frac{g^*_{m'n'}(r_f,\varphi_f;r_c,\varphi_c)}{\Psi_{mn}+\psi^*_{m'n'}}\right]=1, \tag{4.3}$$

with the abbreviation

$$C(\Psi_{mn}) = \mathrm{i}\Psi_{mn}(1-\mathrm{e}^{\mathrm{i}\Psi_{mn}T_{MN}})\left[\frac{\mathrm{e}^{-\mathrm{i}\phi}}{\Psi_{mn}-(2\pi/T_{MN})}+\frac{\mathrm{e}^{\mathrm{i}\phi}}{\Psi_{mn}+(2\pi/T_{MN})}\right]. \tag{4.4}$$

The asterisk denotes the complex conjugate. This equation can be solved numerically (for example, with the Newton/Raphson method).

4.2. RAIL VERSION OF THE ACTIVE CONTOL SYSTEM

The linear dependence of the friction force on the difference between wheel and rail velocity is expressed by the friction characteristic

$$F_f = F_0 + \gamma(v_w - v_r). \tag{4.5}$$

This is substituted into equation (2.6), and again a linear integral equation for v_w is obtained. The complex eigenfrequencies Ψ_{mn} are the roots of the following set of non-linear algebraic equations (see Appendix A):

$$\gamma\left(\Psi_{mn}-\frac{\alpha}{T_{MN}}C(\Psi_{mn})\right)$$

$$\times\frac{1}{2}\sum_{m'=0}^{\mu}\sum_{n'=1}^{\nu}\left[\frac{g_{m'n'}(r_f,\varphi_f;r_f,\varphi_f)}{\Psi_{mn}-\psi_{m'n'}}+\frac{g^*_{m'n'}(r_f,\varphi_f;r_f,\varphi_f)}{\Psi_{mn}+\psi^*_{m'n'}}\right]=1, \tag{4.6}$$

where the abbreviation $C(\Psi_{mn})$ is given by equation (4.4).

5. ENERGY CONSIDERATIONS FOR SINGLE-MODE WHEELS

In this section, the wheel is modelled as a single-degree-of-freedom oscillator, with frequency ω_{MN}, which is also the frequency set at the filter; damping is neglected. This is a rather crude approach, but it allows a purely analytical treatment that gives insight into the physics of the active control system. The basis is the oscillatory energy supplied to the wheel by the friction force and by the control system. Again, the friction characteristic is assumed to be linear.

5.1. WHEEL VERSION OF THE ACTIVE CONTROL SYSTEM

The average energy change ΔE, caused by the friction force (at point (r_f, φ_f)) and the control force (at point (r_c, φ_c)), is

$$\Delta E = \overline{F_f(t) v_w(r_f, \varphi_f, t)} + \overline{F_c(t) v_w(r_c, \varphi_c, t)}. \tag{5.1}$$

The overbar denotes the time average over one period of the oscillation. This average energy change is an indicator for the stability of the wheel: the oscillation is stable if $\Delta E < 0$, and unstable if $\Delta E > 0$. The wheel velocity at point (r_f, φ_f) is taken to be

$$v_w(r_f, \varphi_f, t) = v_{MN} \cos \omega_{MN} t. \tag{5.2}$$

The point (r_c, φ_c) is taken to be on the wheel edge opposite to the point (r_f, φ_f) (see Figure 3), so that the wheel velocity at that point can be stated from symmetry considerations. As Figure 3 shows, the wheel oscillation is in phase for even azimuthal mode numbers M (number of nodal lines), and out of phase for odd M; therefore,

$$v_w(r_c, \varphi_c, t) = \begin{cases} v_{MN} \cos \omega_{MN} t & \text{if } M \text{ is even,} \\ -v_{MN} \cos \omega_{MN} t & \text{if } M \text{ is odd.} \end{cases} \tag{5.3}$$

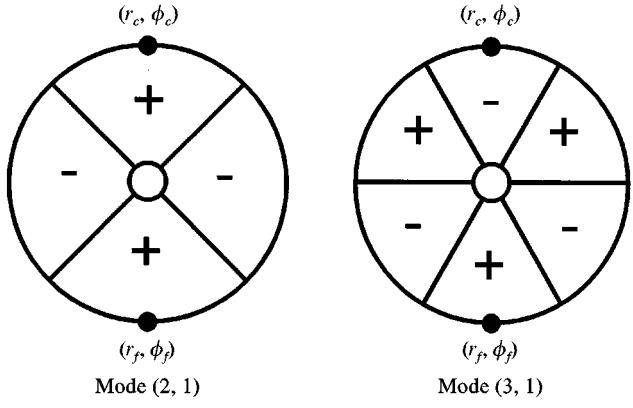

Figure 3. Examples of modes with even and odd azimuthal mode numbers M: (a) $M = 2$; (b) $M = 3$.

The time history of the friction force is obtained from a combination of equations (4.2) and (5.2) to give

$$F_f(t) = F_0 + \gamma v_{MN} \cos \omega_{MN} t. \tag{5.4}$$

The control force, which is a phase-shifted and amplified version of the wheel velocity at (r_f, φ_f), has the time history

$$F_c(t) = \alpha v_{MN} \cos(\omega_{MN} t - \phi). \tag{5.5}$$

Substitution of equations (5.2)–(5.5) into equation (5.1) gives the average energy change

$$\Delta E = \gamma v_{MN}^2 \tfrac{1}{2} \left(1 \pm \frac{\alpha}{\gamma} \cos \phi \right), \tag{5.6}$$

where the upper sign is for even mode numbers M, and the lower sign for odd M. The wheel oscillation is

$$\begin{array}{ll} \text{stable} & 1 \pm \dfrac{\alpha}{\gamma} \cos \phi < 0, \\ & \text{if} \\ \text{unstable} & 1 \pm \dfrac{\alpha}{\gamma} \cos \phi > 0. \end{array} \tag{5.7}$$

The inequalities in equation (5.7) describe two areas, one of stability and one of instability, in the $\alpha\phi$-plane. The boundary between these two areas is given by the curve

$$1 \pm \frac{\alpha}{\gamma} \cos \phi = 0, \tag{5.8}$$

or, in explicit form

$$\alpha = \begin{cases} \gamma / \cos(\phi - \pi) & \text{if } M \text{ is even,} \\ \gamma / \cos \phi & \text{if } M \text{ is odd.} \end{cases} \tag{5.9}$$

They are both U-shaped curves with a maximum width of π, and a minimum at $\alpha = \gamma$ (see Figure 4(a) and (b)). Similar U-shaped curves have been found by Ffowcs Williams and Huang [11] for the control of compressor surge.

5.2. RAIL VERSION OF THE ACTIVE CONTROL SYSTEM

The average energy change ΔE caused by the friction force, which is affected by the control system, is given by

$$\Delta E = \overline{F_f(t) v_w(r_f, \varphi_f, t)}. \tag{5.10}$$

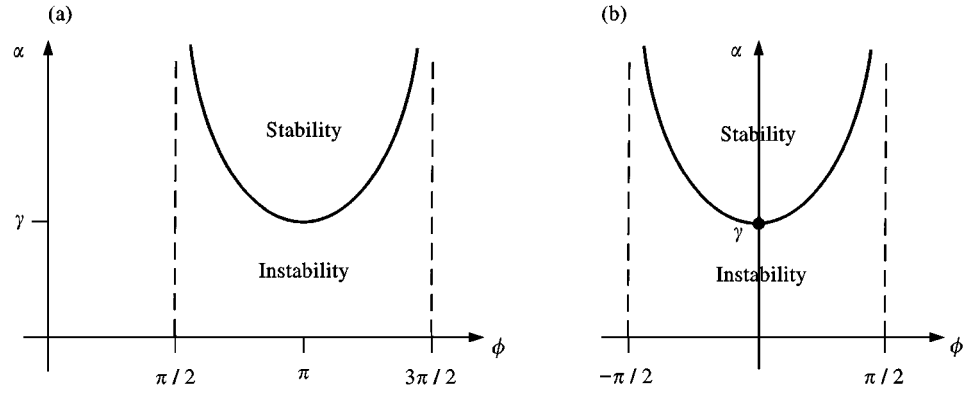

Figure 4. Stability map of a single-mode wheel: (a) even azimuthal mode number M; (b) odd azimuthal mode number M.

The wheel velocity is given by equation (5.2). The control signal here is the rail velocity, which is a phase-shifted and amplified version of the wheel velocity, hence

$$v_r(t) = \alpha v_{MN} \cos(\omega_{MN} t - \phi). \tag{5.11}$$

The time history of the friction force can then be obtained by substituting equations (5.2) and (5.11) into equation (4.5),

$$F_f(t) = F_0 + \gamma v_{MN}[\cos \omega_{MN} t - \alpha \cos(\omega_{MN} t - \phi)]. \tag{5.12}$$

With equations (5.2) and (5.12), the average energy change (5.10) becomes

$$\Delta E = \gamma v_{MN}^2 \tfrac{1}{2}(1 - \alpha \cos \phi); \tag{5.13}$$

this holds for all mode numbers. The wheel oscillation is

$$\begin{array}{ll} \text{stable} & 1 - \alpha \cos \phi < 0, \\ \text{if} & \\ \text{unstable} & 1 - \alpha \cos \phi > 0. \end{array} \tag{5.14}$$

Again, these inequalities describe an area of stability and one of instability in the $\alpha\phi$-plane. The boundary between these areas is given by the curve

$$\alpha = \frac{1}{\cos \phi}. \tag{5.15}$$

This, too, is a U-shaped curve in the $\alpha\phi$-plane with a maximum width of π. It is centred around $\phi = 0$. The minimum value of α is at $\alpha = 1$.

The performance of the two versions of the active control system is very similar. Both are insensitive to errors in phase-shift and amplification: the phase-shift just

needs to be in a certain range (of width up to π), and the amplification needs to be above a certain minimum value.

6. NUMERICAL RESULTS

The equations in Sections 3 and 4 were solved numerically for a small model wheel, shaped like a flat circular disc with a hub at the centre. It was made from steel with the following material properties: $\rho = 8000\ \mathrm{kg/m^3}$ (mass density), $E = 2 \times 10^{11}\ \mathrm{N/m^2}$ (Young's modulus), $\nu = 0{\cdot}3$ (Poisson ratio), and had the following geometry: $d = 0{\cdot}003$ m (wheel thickness), $a = 0{\cdot}038$ m (wheel radius), $b = 0{\cdot}01$ m (radius of wheel hub).

Parameters describing the (linear) friction characteristic were: $\gamma = 15000\ \mathrm{N\,s/m}$ (slope of the slip section), $F_0 = 1{\cdot}07$ N (mean part of the friction force for small velocities).

Parameters describing the control system were $(r_f, \varphi_f) = (a, 0)$ (point where the friction force acts), $(r_c, \varphi_c) = (a, \pi)$ (point where the control force acts for wheel version). The amplification α, phase-shift ϕ, and filter frequency ω_{MN} were varied within wide ranges.

Only the first 5 modes were considered in the calculations. The properties of the free wheel (no friction, no control) are shown in Table 1.

TABLE 1

Eigenfrequencies ω_{mn} and the Green's function amplitudes g_{mn} of the considered modes (free wheel)

m	n	ω_{mn} $(2\pi\,\mathrm{s}^{-1})$	real g_{mn}	imag g_{mn} $(10^{-9}$ m/N s) $(r_f, \varphi_f; r_f, \varphi_f)$	imag g_{mn} $(10^{-9}$ m/N s) $(r_f, \varphi_f; r_c, \varphi_c)$
0	1	3020	0	1969	1969
1	1	2922	0	4124	−4124
2	1	3655	0	3472	3472
3	1	6482	0	2141	−2141
4	1	10 980	0	1409	1409

The growth rates δ_{mn} of the free wheel were varied by choosing different sets of modal loss factors. The value of δ_{mn} for a particular mode (m, n) is an important parameter for the stability behaviour of that mode (see reference [5]). By varying δ_{mn}, one can simulate wheels with different combinations of stable and unstable modes, and examine the performance of the control system operating under these conditions.

6.1. WHEEL VERSION OF THE ACTIVE CONTROL SYSTEM

The motion of the controlled friction-driven wheel was analyzed with the two methods described in Sections 3.1 and 4.1. The time history of the wheel velocity

was calculated with the iteration scheme of equations (3.2) and (3.3). During the early stages of the time history, the control was absent, and it was switched on after several periods of the oscillation. An example of a calculated time history is shown in Figure 5. The solid curve gives the wheel velocity $v_w(r_f, \varphi_f, t)$, the curve with the long dash gives the friction force, $F_f(t)$, and the curve with the short dash gives the control force, $F_c(t)$.

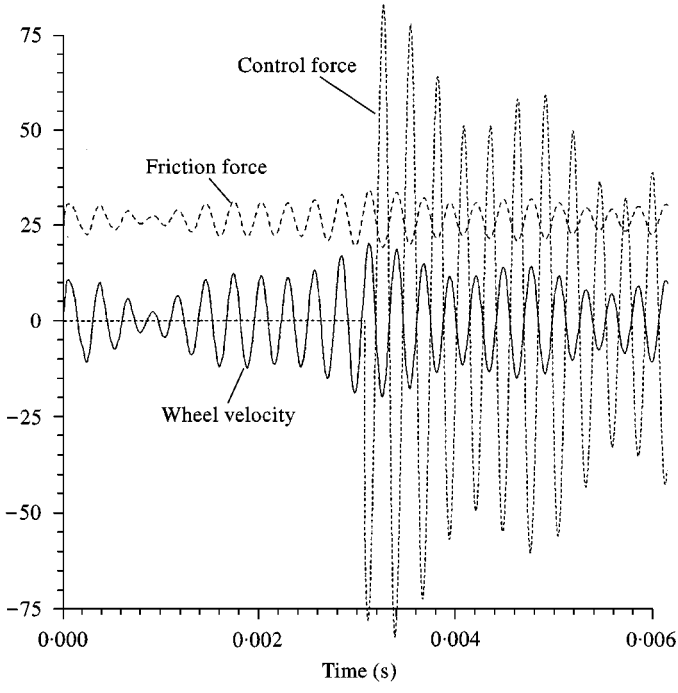

Figure 5. Active control of the unstable mode (2, 1). The co-ordinate labels along the vertical axis apply to the velocity (in 10^{-6} m/s), but not to the forces. The friction force and control force are displayed with the same scale.

The control parameters used to produce this figure were: $\phi = \pi$ (phase-shift), $\alpha = 1{\cdot}1\gamma$ (amplification), $\omega_{MN} = 2\pi \cdot 3655\ \mathrm{s}^{-1}$ (filter frequency, tuned to mode (2, 1)).

This is a case where the control is successful. Mode (2, 1) is unstable, and its exponential growth can be seen in the first half of the time history during which there is no control. The control system is switched on at a time about halfway along the displayed time interval. The control force amplitude rapidly reaches a very large value, but then decreases exponentially, together with the velocity amplitude, during the second half of the displayed time interval.

More precise stability predictions, corroborating those from the time history calculation, can be made from the eigenfrequency calculation for the friction-driven wheel. Equation (4.3) was solved numerically to give the complex eigenfrequencies Ψ_{mn}. Their real parts Ω_{mn} and imaginary parts Δ_{mn} are listed in Table 2 for the case without control and with control (control parameters as above). Modes with negative Δ_{mn} are stable.

TABLE 2

Eigenfrequencies Ω_{mn} and growth rates Δ_{mn} of the friction-driven wheel (without and with control). The growth rates δ_{mn} of the free wheel are also listed

			Without control		With control	
m	n	δ_{mn} (s^{-1})	Ω_{mn} ($2\pi\,s^{-1}$)	Δ_{mn} (s^{-1})	Ω_{mn} ($2\pi\,s^{-1}$)	Δ_{mn} (s^{-1})
0	1	−1328	2993	−1198	3010	−1415
1	1	−1285	2975	−599	2976	−98
2	1	−138	3637	498	3657	−221
3	1	−2859	6480	−2200	6466	−2596
4	1	−4829	10 979	−4103	10 947	−4108

A large number of simulations with different control parameters and different modal loss factors have been performed. The findings are summarized below.

If mode (M, N) is unstable, and the control system is tuned to that mode, then the optimal phase-shift to control that mode is $\phi = 0$ if M is odd, and $\phi = \pi$ if M is even. This is not surprising in the light of the stability predictions in Section 5 for an isolated mode.

The presence of other modes (whether stable or unstable without control) has a negative effect on the optimistic predictions of Section 5. The phase range, where stability can be achieved for *all* modes, is no longer of width π, but significantly reduced. Also, the amplification needs to be chosen more carefully: it still needs to satisfy $\alpha > \gamma$, but with growing α-values there is an increased risk of previously stable modes becoming unstable. This is because an increase in α enhances the modal coupling brought about by the control system (see Section 2.3).

The modal coupling can work in one's favour if there are several unstable modes: the control system can be tuned to only one of them, but careful choice of the control parameters may control the other modes. One such example is shown in Table 3. The control system parameters were: $\phi = 0{\cdot}3\pi$, $\alpha = 2\gamma$, $\omega_{MN} = 2\pi{\cdot}6482\ s^{-1}$ (filter frequency, tuned to mode (3, 1)).

TABLE 3

Eigenfrequencies Ω_{mn} and growth rates Δ_{mn} of the friction-driven wheel (without and with control). The growth rates δ_{mn} of the free wheel are also listed

			Without control		With control	
m	n	δ_{mn} (s^{-1})	Ω_{mn} ($2\pi\,s^{-1}$)	Δ_{mn} (s^{-1})	Ω_{mn} ($2\pi\,s^{-1}$)	Δ_{mn} (s^{-1})
0	1	−1328	2993	−1198	3031	−1338
1	1	−1285	2975	−599	2913	−77
2	1	−184	3637	449	3756	−273
3	1	−244	6473	411	6295	−371
4	1	−4829	10 979	−4105	10 844	−4284

Here, modes (2, 1) and (3, 1), which were unstable before the control, are stabilized. As the number of unstable modes increases, it becomes more and more difficult to control them all. The following guideline can be given about the choice of the control frequency ω_{MN}, if there are two (or more) unstable modes to be controlled. The control is more likely to succeed, if it is tuned to the mode with the highest unstable frequency; this tends to minimize contamination effects similar to aliasing.

A very difficult case to control is the one where there is one unstable mode and one mode that is marginally stable and has a higher frequency. The control system can only be tuned to the unstable mode, but it may be impossible to avoid exciting the marginally stable mode, no matter how the control parameters are chosen.

6.2. RAIL VERSION OF THE ACTIVE CONTROL SYSTEM

This version of the control system was studied with the methods described in Sections 3.2 and 4.2. The iteration scheme of equations (3.6) and (3.7) gave the time history of the wheel velocity, and the numerical solution of equation (4.6) gave the complex eigenfrequencies of the actively-controlled, friction-driven wheel. Again, a large number of simulations have been carried out to study the performance of this version of the control system and to compare it with the other version.

The optimal phase-shift to control a particular mode (M, N) is $\phi = 0$ for all (M, N). The minimum amplification is $\alpha = 1$. The range of α- and ϕ-values that give stability for the controlled mode is very large and similar to the range found in section 5.2 for an isolated mode. However, this version of the control system, too, introduces coupling between the modes and affects the stability of the other modes. Thus, the range of α- and ϕ-values that give stability, not just for the controlled mode but for *all* modes, is very much reduced and may be non-existent. Again, a beneficial side-effect of this modal coupling is the possibility of controlling two (or more) unstable modes simultaneously. In such a case, the control system is best tuned to the unstable mode that has the highest frequency.

We also studied the performance of the control system under non-linear conditions, i.e., when the wheel oscillation has reached a stick/slip limit-cycle oscillation. The time history for such a case is shown in Figure 6. A piecewise linear friction characteristic (see Figure 3(b) in reference [5]) was used with the following parameters:

$$\gamma = 15\,000 \text{ N s/m} \quad \text{(slope of the slip section)},$$

$$\Gamma = -\,100\,000 \text{ N s/m} \quad \text{(slope of the stick section)},$$

$$V = 50 \times 10^{-6} \text{ m/s} \quad \text{(crabbing speed, i.e. transition from slip to stick motion)},$$

$$F_0 = 1{\cdot}07 \text{ N (mean part of the friction force for small velocities)}.$$

The velocity of the uncontrolled wheel is shown in the first two-thirds of the displayed time history (solid line). The motion starts with an unstable amplitude

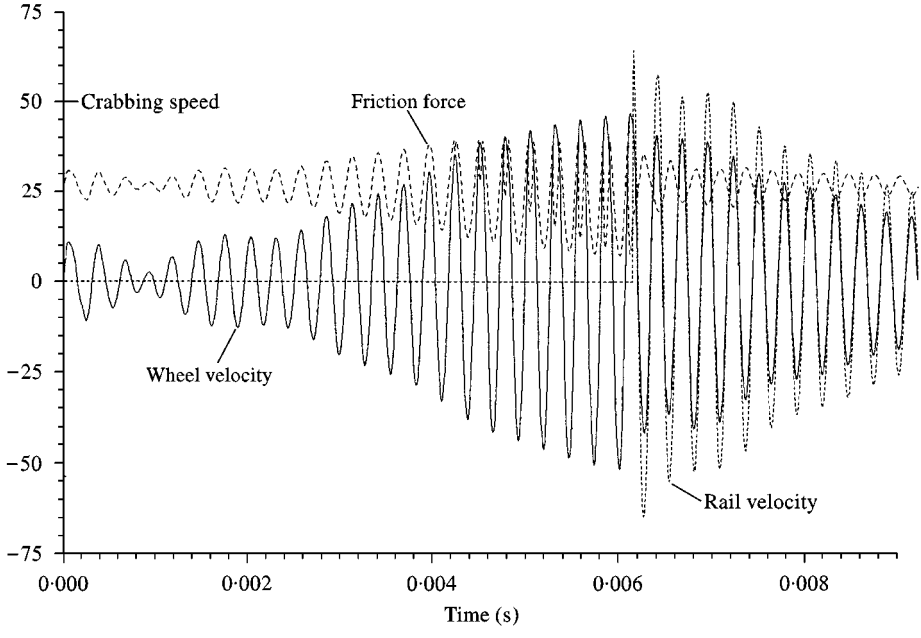

Figure 6. Active control of a limit-cycle oscillation. The co-ordinate labels along the vertical axis apply to the wheel velocity and rail velocity (in 10^{-6} m/s), but not to the friction force.

growth; during this stage the wheel performs an oscillatory slip-only motion. When the velocity amplitude reaches the crabbing speed, an oscillatory stick/slip motion sets in. This is a limit-cycle oscillation with a velocity amplitude given by the crabbing speed V; the wheel is now driven by a non-linear friction force. The start-up of the control system is during this limit-cycle oscillation, at time 0·006 s. The control parameters are: $\phi = 0$ (phase-shift), $\alpha = 1{\cdot}3$ (amplification), $\omega_{MN} = 2\pi \cdot 3655\,\mathrm{s}^{-1}$ (filter frequency, tuned to mode (2, 1)).

The amplitude starts to decay and quickly reaches levels where the friction force becomes linear again. Table 4 gives the corresponding linear data from the eigenfrequency calculation and lists the frequencies and growth rates of the wheel without and with control.

TABLE 4

Eigenfrequencies Ω_{mn} and growth rates Δ_{mn} of the friction-driven wheel (without and with control). The growth rates δ_{mn} of the free wheel are also listed

			Without control		With control	
m	n	δ_{mn} (s^{-1})	Ω_{mn} ($2\pi\,\mathrm{s}^{-1}$)	Δ_{mn} (s^{-1})	Ω_{mn} ($2\pi\,\mathrm{s}^{-1}$)	Δ_{mn} (s^{-1})
0	1	−1328	2993	−1198	3000	−1324
1	1	−1258	2975	−599	2819	−1085
2	1	−115	3637	520	3651	−323
3	1	−2851	6480	−2200	6492	−1812
4	1	−4829	10979	−4103	10943	−4127

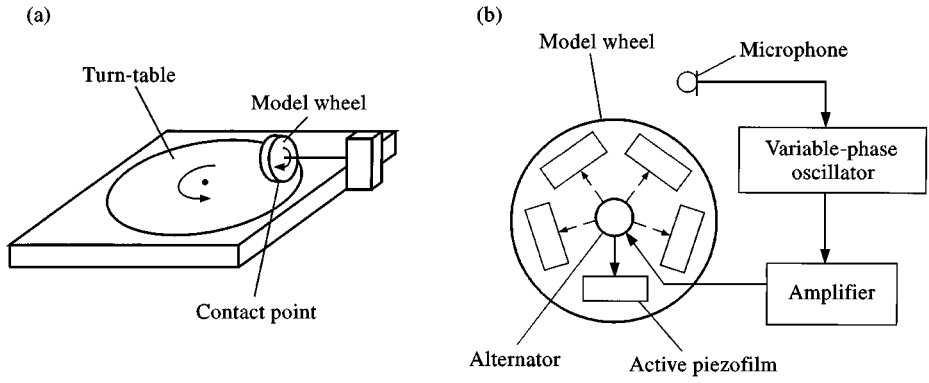

Figure 7. Model rig to simulate: (a) wheel crabbing, and (b) its active control.

The wheel version of the active control system has also been found to work under non-linear conditions. For example, the limit-cycle oscillation in Figure 6 can be suppressed by a contol system with the parameters $\phi = \pi$, $\alpha = 1{\cdot}3\,\gamma$, $\omega_{MN} = 2\pi \cdot 3655\ \mathrm{s}^{-1}$ (filter frequency, tuned to mode (2, 1)).

7. EXPERIMENTAL RIG

The experimental rig, shown schematically in Figure 7(a), simulates curve squeal produced by wheel crabbing. The model wheel is a flat circular steel disc with a hub at the centre. Its measurements are given in Section 6. It is held by an axle at the centre, allowed to rotate, and rolls on the turntable of an old record player, which represents the rail.

The angle between the plane of the wheel and the tangent to the wheel's circular path on the turntable can be varied smoothly between -45 and $45°$. If this angle is zero, i.e., if the wheel is aligned tangentially with its circular path, there is no friction force perpendicular to the wheel, and no squeal noise is heard. For all other angles, the friction force does have a perpendicular component, and this gives rise to squeal noise. The normal load acting on the wheel can also be varied; this is done with a vertical compression spring pressing down on the wheel axle. This normal load needs to have a minimum value for squeal to be produced; the intensity of the squeal increases with increasing normal load. The wheel squeals at a single frequency of about 6800 Hz, which is that of mode (3, 1). The frequency spectrum of the squeal noise is shown in Figure 8.

The active control system, shown in Figure 7(b), was applied to the wheel. It had the following components. A microphone picked up the squeal noise. The microphone signal was fed into a variable-phase oscillator (model VPO 602, from Feedback) that had the dual role of narrowband filter and phase-shifter. It generated a phase-shifted single-frequency signal relative to its input signal, and had to be "tuned in" to the frequency of the squeal. The oscillator output was fed

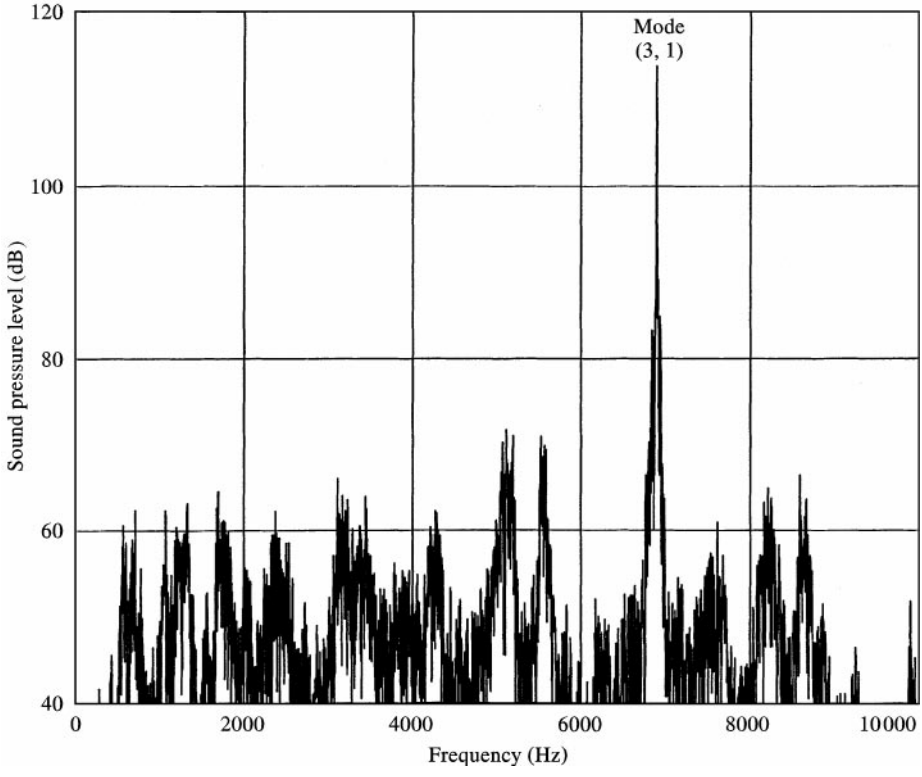

Figure 8. Frequency spectrum of the squeal noise.

into an amplifier (120 W power slave amplifier, type US4, from ILP electronics), and its output gave the control signal.

The transducer to apply the control force was a piezo-film actuator (type DT1-052K, from Elf Atochem) attached with double-sided tape to the wheel. The film was excited by the control signal to perform an in-plane motion (shrinking and stretching with the frequency of the squeal), and this forced bending oscillations in the wheel. The wheel was rotating, and in order to keep the point of the control force reasonably stationary relative to the point of the friction force, the following arrangement was designed. Five identical piezo-films were attached along a ring close to the outer edge of the wheel (see Figure 7(b)), but only one of them, the one closest to the contact point with the turntable, was active. An alternator (in line with the axle of the wheel) with a brush was used to switch the control signal from one piezo-film to the next as the wheel was rotating.

The squeal noise could be controlled, and even completely annulled, with this model control system. However, it was rather unreliable, and only worked for squeal noise of a low intensity. This weakness was not due to the method in principle, but to the delicacy of the piezo-films used. Although they were driven at (and beyond) their power limits, they were often not strong enough to deliver the required control force amplitudes. Nevertheless, we have experimentally verified that curve squeal can be suppressed by an active control system.

8. CONCLUSIONS

The squeal noise that is produced by trains traversing a curve is due to unstable bending oscillations of individual train wheels. These oscillations can be suppressed by a special form of active control. A sensor picks up the wheel's bending velocity (or a measure of it) and passes it to a narrow-band filter tuned to the squeal frequency (or one of the squeal frequencies if there are several peaks in the spectrum). The output signal, which is a single-frequency signal, is then phase-shifted and amplified. The resulting control signal drives an actuator, which may be attached to the wheel or to the rail. Both versions of the active control system were studied theoretically by a detailed mathematical model that was used for numerical simulations. According to these simulations, which were performed for a model wheel with several bending modes, both versions can achieve total control of the squeal noise, even when the phase-shift and amplification deviate from the optimum values.

A feature of this control system is that it can be tuned to the frequency of only one bending mode, yet it causes coupling between all modes. The mode coupling is usually detrimental in that it can destabilize previously stable modes. Care has to be taken to find values for phase-shift and amplification that give control of all modes. This becomes difficult if the squealing wheel has marginally stable modes in addition to the one that is to be controlled. It may even be impossible in such cases to achieve control for all wheel modes. The easiest case to control is that of a wheel with one unstable mode amongst firmly stable modes. On the other hand, the modal coupling can be beneficial and control two simultaneously unstable modes by tuning the control to one of them, usually the one with the higher frequency.

The active control system works for all amplitude ranges of the oscillating wheel and can operate under linear and non-linear conditions. In the early, linear, stages of an instability, when the wheel oscillates with small, but increasing, amplitude, the control system can reverse the amplitude increase, thus preventing the build-up of a high-intensity squeal noise. During a high-intensity squeal noise, the wheel performs a limit-cycle oscillation with a large amplitude and is, mathematically speaking, driven non-linearly. Even in this situation, the active control system can be applied successfully to bring about a swift amplitude decay.

The energy requirements of the active control system are not constant but decay with the amplitude of the wheel oscillation. The requirements are high initially if a fully developed squeal is to be suppressed. They are considerably smaller if the active control system operates on an ongoing basis, ready to quash an instability as soon as it becomes detectable.

The theoretically predicted effectiveness of our active contol system has been confirmed experimentally by a small-scale model rig, representing the wheel version. A more robust rig would demonstrate its effectiveness in the harsh environment of train wheels and rails. It would also allow research into other friction-related questions, such as whether the active control reduces the wear that wheels suffer during curve negotiation.

An extension (which involves a little more technology) of our active control method would be a branched feedback loop, which controls each mode of the squealing wheel individually. The signal from the sensor would be divided up into

the modal components; these are individually phase-shifted and amplified, and subsequently combined to be fed into the actuator. It is likely that this branched active control system is immune against unwanted interference between the modes, making it easier to achieve control for all modes of the squealing wheel.

ACKNOWLEDGMENTS

We are grateful to Mike Davies and Mike Wallace of the Keele Electronics Workshop for their help and advice with building the squeal rig. We are also grateful to William Kirk for producing the figures. The research described in this paper was supported by the Engineering and Physical Sciences Research Council of the UK (EPSRC grant number GR/H73776).

REFERENCES

1. M. Hecht 1995 *Schweizer Eisenbahn-Revue* **3**, 102–108. Kurvenkreischen-Ursachen und Gegenmassnahmen.
2. H. von Stappenbeck 1954 *Zeitschrift VDI* **96**, 171–175. Das Kurvengeräusch der Strßenbahn-Möglichkeiten zu seiner Unterdrückung.
3. M. J. Rudd 1976 *Journal of Sound and Vibration* **46**, 381–394. Wheel/rail noise—Part II: wheel squeal.
4. P. J. Remington 1985 *Journal of Sound and Vibration* **116**, 339–353. Wheel/rail squeal and impact noise: What do we know? What don't we know? Where do we go from here?
5. Maria A. Heckl and I. D. Abrahams 2000 *Journal of Sound and Vibration* **229**, 669–693. Curve squeal of train wheels, Part 1: Mathematical model for its generation.
6. E. Schneider, K. Popp and H. Irretier 1988 *Journal of Sound and Vibration* **120**, 227–244. Noise generation in railway wheels due to rail-wheel contact forces.
7. U. Fingberg 1990 *Journal of Sound and Vibration* **143**, 365–377. A model of wheel-rail squealing noise.
8. F. Périard 1998 *Ph.D. Dissertation, Technische Universiteit Delft*; ISBN 90-9011964-7, *NUGI* 834. Wheel-rail noise generation: curve squealing by trams.
9. M. A. Heckl 1988 *Journal of Sound and Vibration* **124**, 117–133. Active control of the noise from a Rijke tube.
10. X. Y. Huang 1987 *AIAA Journal* **25**, 1126–1132. Active control of aerofoil flutter.
11. J. E. Ffowcs Williams and X. Y. Huang 1989 *Journal of Fluid Mechanics* **204**, 245–262. Active stabilisation of compressor surge.
12. M. A. Heckl and I. D. Abrahams 1996 *Journal of Sound and Vibration* **193**, 417–426. Active control of friction-driven oscillations.
13. M. A. Heckl 2000 *Journal of Sound and Vibration* **229**, 695–707. Curve squeal of train wheels, Part 2: Which wheel modes are prone to squeal?

APPENDIX A: DERIVATION OF THE EQUATION FOR THE COMPLEX EIGENFREQUENCIES OF THE CONTROLLED FRICTION-DRIVEN WHEEL

We restrict our considerations to a wheel with a finite number of modes,

$$m = 0, \ldots, \mu, \quad n = 1, \ldots, \nu. \tag{A1}$$

Its Green's function, or displacement response to an impulse force at point (r_f, φ_f) at time t', is then given by equation (2.2a) with its sums truncated; to allow the subsequent manipulations, the real part of the complex term is expressed as half the sum of the complex term and its complex conjugate,

$$G(r, \varphi; r_f, \varphi_f; t - t') = \frac{1}{2} \sum_{m=0}^{\mu} \sum_{n=1}^{\nu} (g_{mn}(r, \varphi; r_f, \varphi_f) e^{-i\psi_{mn}(t-t')} + g^*_{mn}(r, \varphi; r_f, \varphi_f) e^{i\psi^*_{mn}(t-t')}). \tag{A2}$$

By analogy, the displacement $w(t)$ of the controlled friction-driven wheel at point (r_f, φ_f) is also written as a superposition of modes,

$$w(t) = \frac{1}{2}\left[w_0 + w_0^* + \sum_{m=0}^{\mu} \sum_{n=1}^{\nu} (w_{mn} e^{-i\Psi_{mn} t} + w^*_{mn} e^{i\Psi^*_{mn} t}) \right]. \tag{A3}$$

The complex frequencies Ψ_{mn}, the corresponding complex amplitudes w_{mn}, and the constant term w_0 are unknown at this stage and will be determined from the governing equations (2.3) and (2.6) respectively for versions 1 and 2 of the active control system.

The velocity corresponding to the displacement $w(t)$ is

$$v_w(r_f, \varphi_f, t) = \dot{w}(t), \tag{A4}$$

hence, by differentiation of equation (A3),

$$v_w(r_f, \varphi_f, t) = \frac{1}{2} \sum_{m=0}^{\mu} \sum_{n=1}^{\nu} (-i\Psi_{mn} w_{mn} e^{-i\Psi_{mn} t} + i\Psi^*_{mn} w^*_{mn} e^{i\Psi^*_{mn} t}). \tag{A5}$$

The control signal amplitude $A_{MN}(t')$, given by equation (2.9), can also be written as a modal superposition by substituting for $v_w(r_f, \varphi_f, t)$ with equation (A5) and evaluating the integral over t; the result is

$$A_{MN}(t') = \frac{1}{T_{MN}} \sum_{m=0}^{\mu} \sum_{n=1}^{\nu} \left[\frac{\Psi_{mn} w_{mn}}{\Psi_{mn} - (2\pi/T_{MN})} (1 - e^{i\Psi_{mn} T_{MN}}) e^{i(-\Psi_{mn} + (2\pi/T_{MN}))t'} + \frac{\Psi^*_{mn} w^*_{mn}}{\Psi^*_{mn} + (2\pi/T_{MN})} (1 - e^{-i\Psi^*_{mn} T_{MN}}) e^{i(\Psi^*_{mn} + (2\pi/T_{MN}))t'} \right]. \tag{A6}$$

A.1. WHEEL VERSION OF THE ACTIVE CONTROL SYSTEM

The governing equation (2.3) is evaluated at point (r_f, φ_f), and the velocity on the left-hand side is replaced by the displacement derivative, according to (A4). The

t-dependence of the resulting equation is in terms of t-derivatives (indicated by dots) only; the equation can thus be integrated with respect to time t, to give

$$w(t) = \int_{t'=0}^{t} (F_f[v_w(r_f, \varphi_f, t')]\, G(r_f, \varphi_f; r_f, \varphi_f; t - t') + F_c(t')\, G(r_f, \varphi_f; r_c, \varphi_c; t - t'))\, \mathrm{d}t'. \tag{A7}$$

The integration constant is ignored as there is a constant term, $\frac{1}{2}(w_0 + w_0^*)$, included in the expression (A3) for the wheel displacement. Equation (A7) is an integrodifferential equation of the Volterra type for the displacement of the controlled, friction-driven wheel. It is solved by expressing all functions of t and t' by modal superpositions. Expression (A3) is substituted into the left-hand side of equation (A7). Substituted into the right-hand side of equation (A7) are: (i) the linear friction characteristic (4.2) with equation (A5) for the wheel velocity, (ii) the control force (2.5) (real part replaced by the usual expression involving the complex conjugate) with equation (A6) for the control signal amplitude $A_{MN}(t')$ (the expression for F_c can be simplified with $\mathrm{e}^{\pm \mathrm{i}(-\omega_{MN} + (2\pi/T_{MN}))} = 1$), and (iii) the Green's function (A2) evaluated at the points (r_f, φ_f) and (r_c, φ_c). The resulting equation is

$$\begin{aligned}
&\frac{1}{2}\left[w_0 + w_0^* + \sum_{m=0}^{\mu} \sum_{n=1}^{\nu} (w_{mn} \mathrm{e}^{-\mathrm{i}\Psi_{mn} t} + w_{mn}^* \mathrm{e}^{\mathrm{i}\Psi_{mn}^* t}) \right] \\
&\quad = \int_0^t \left[F_0 + \gamma \frac{1}{2} \sum_{m=0}^{\mu} \sum_{n=1}^{\nu} (-\mathrm{i}\Psi_{mn} w_{mn} \mathrm{e}^{-\mathrm{i}\Psi_{mn} t'} + \mathrm{i}\Psi_{mn}^* w_{mn}^* \mathrm{e}^{\mathrm{i}\Psi_{mn}^* t'}) \right] \\
&\qquad \times \left[\frac{1}{2} \sum_{m'=0}^{\mu} \sum_{n'=0}^{\nu} (g_{m'n'}^{(f)} \mathrm{e}^{-\mathrm{i}\psi_{m'n'}(t-t')} + g_{m'n'}^{(f)*} \mathrm{e}^{\mathrm{i}\psi_{m'n'}^*(t-t')}) \right] \mathrm{d}t' \\
&\qquad + \int_0^t \frac{\alpha}{T_{MN}} \frac{1}{2} \sum_{m=0}^{\mu} \sum_{n=1}^{\nu} \left[\Psi_{mn} w_{mn} \left(\frac{\mathrm{e}^{-\mathrm{i}\phi}}{\Psi_{mn} - (2\pi/T_{MN})} + \frac{\mathrm{e}^{\mathrm{i}\phi}}{\Psi_{mn} + (2\pi/T_{MN})} \right) \right. \\
&\qquad \times (1 - \mathrm{e}^{\mathrm{i}\Psi_{mn} T_{MN}}) \mathrm{e}^{-\mathrm{i}\Psi_{mn} t'} \\
&\qquad \left. + \Psi_{mn}^* w_{mn}^* \left(\frac{\mathrm{e}^{-\mathrm{i}\phi}}{\Psi_{mn}^* + (2\pi/T_{MN})} + \frac{\mathrm{e}^{\mathrm{i}\phi}}{\Psi_{mn}^* - (2\pi/T_{MN})} \right) (1 - \mathrm{e}^{-\mathrm{i}\Psi_{mn}^* T_{MN}}) \mathrm{e}^{\mathrm{i}\Psi_{mn}^* t'} \right] \\
&\qquad \times \left[\frac{1}{2} \sum_{m'=0}^{\mu} \sum_{n'=1}^{\nu} (g_{m'n'}^{(c)} \mathrm{e}^{-\mathrm{i}\psi_{m'n'}(t-t')} + g_{m'n'}^{(c)*} \mathrm{e}^{\mathrm{i}\psi_{m'n'}^*(t-t')}) \right] \mathrm{d}t',
\end{aligned} \tag{A8}$$

where the following abbreviations have been used for the Green's function amplitudes:

$$g_{m'n'}(r_f, \varphi_f; r_f, \varphi_f) = g_{m'n'}^{(f)}, \tag{A9a}$$

$$g_{m'n'}(r_f, \varphi_f; r_c, \varphi_c) = g_{m'n'}^{(c)}. \tag{A9b}$$

A number of lengthy, by straightforward, manipulations follow, which are not shown here. They include: multiplying out the brackets in the integrand, putting the t-dependent terms outside the integral, performing the integration over the t'-dependent terms to obtain new t-dependent terms, multiplying both sides of the equation by 2, and sorting the terms on the right-hand side into constant terms and terms with factors $e^{-i\Psi_{mn}t}$, $e^{i\Psi^*_{mn}t}$, $e^{-i\psi_{m'n'}t}$, $e^{i\psi^*_{m'n'}t}$. The final result is

$$
\begin{aligned}
&w_0 + w_0^* + \sum_{m=0}^{\mu}\sum_{n=1}^{\nu}\left(w_{mn}e^{-i\Psi_{mn}t} + w_{mn}^* e^{i\Psi^*_{mn}t}\right)\\
&\quad= \sum_{m'=0}^{\mu}\sum_{n'=1}^{\nu}\left(g^{(f)}_{m'n'}\frac{F_0}{i\psi_{m'n'}} + g^{(f)*}_{m'n'}\frac{F_0}{-i\psi^*_{m'n'}}\right)\\
&\qquad+ \sum_{m=0}^{\mu}\sum_{n=1}^{\nu} e^{-i\Psi_{mn}t}\Psi_{mn}w_{mn}\left\{\frac{1}{2}\gamma\sum_{m'=0}^{\mu}\sum_{n'=1}^{\nu}\left(\frac{g^{(f)}_{m'n'}}{\Psi_{mn}-\psi_{m'n'}} + \frac{g^{(f)*}_{m'n'}}{\Psi_{mn}+\psi^*_{m'n'}}\right)\right.\\
&\qquad+ \frac{1}{2}\frac{\alpha}{T_{MN}}\frac{1}{i}(1-e^{i\Psi_{mn}T_{MN}})\left(-\frac{e^{-i\phi}}{\Psi_{mn}-(2\pi/T_{MN})} - \frac{e^{i\phi}}{\Psi_{mn}+(2\pi/T_{MN})}\right)\\
&\qquad\left.\times\sum_{m'=0}^{\mu}\sum_{n'=1}^{\nu}\left(\frac{g^{(c)}_{m'n'}}{\Psi_{mn}-\psi_{m'n'}} + \frac{g^{(c)*}_{m'n'}}{\Psi_{mn}+\psi^*_{m'n'}}\right)\right\}\\
&\qquad+ \sum_{m=0}^{\mu}\sum_{n=1}^{\nu} e^{i\Psi^*_{mn}t}\Psi^*_{mn}w^*_{mn}\left\{\frac{1}{2}\gamma\sum_{m'=0}^{\mu}\sum_{n'=1}^{\nu}\left(\frac{g^{(f)}_{m'n'}}{\Psi^*_{mn}+\psi_{m'n'}} + \frac{g^{(f)*}_{m'n'}}{\Psi^*_{mn}-\psi^*_{m'n'}}\right)\right.\\
&\qquad+ \frac{1}{2}\frac{\alpha}{T_{MN}}\frac{1}{i}(1-e^{-i\Psi^*_{mn}T_{MN}})\left(\frac{e^{-i\phi}}{\Psi^*_{mn}+(2\pi/T_{MN})} + \frac{e^{i\phi}}{\Psi^*_{mn}-(2\pi/T_{MN})}\right)\\
&\qquad\left.\times\sum_{m'=0}^{\mu}\sum_{n'=1}^{\nu}\left(\frac{g^{(c)}_{m'n'}}{\Psi^*_{mn}+\psi_{m'n'}} + \frac{g^{(c)*}_{m'n'}}{\Psi^*_{mn}-\psi^*_{m'n'}}\right)\right\}\\
&\qquad+ \sum_{m'=0}^{\mu}\sum_{n'=1}^{\nu} e^{-i\psi_{m'n'}t}\left\{g^{(f)}_{m'n'}\left[\frac{-F_0}{i\psi_{m'n'}}\right.\right.\\
&\qquad\left.+ \frac{1}{2}\gamma\sum_{m=0}^{\mu}\sum_{n=1}^{\nu}\left(\frac{\Psi_{mn}w_{mn}}{\psi_{m'n'}-\Psi_{mn}} - \frac{\Psi^*_{mn}w^*_{mn}}{\psi_{m'n'}+\Psi^*_{mn}}\right)\right]\\
&\qquad+ \frac{1}{2}\frac{\alpha}{T_{MN}}\frac{1}{i}g^{(c)}_{mn}\sum_{m=0}^{\mu}\sum_{n=1}^{\nu}\left[\frac{\Psi_{mn}w_{mn}(1-e^{i\Psi_{mn}T_{MN}})}{\psi_{m'n'}-\Psi_{mn}}\right.\\
&\qquad\left.\times\left(-\frac{e^{-i\phi}}{\Psi_{mn}-(2\pi/T_{MN})} - \frac{e^{i\phi}}{\Psi_{mn}+(2\pi/T_{MN})}\right)\right.
\end{aligned}
$$

$$-\frac{\Psi^*_{mn} w^*_{mn}(1-\mathrm{e}^{-\mathrm{i}\Psi^*_{mn}T_{MN}})}{\mathrm{i}(\psi_{m'n'}+\Psi^*_{mn})}\left(\frac{\mathrm{e}^{-\mathrm{i}\phi}}{\Psi^*_{mn}+(2\pi/T_{MN})}+\frac{\mathrm{e}^{\mathrm{i}\phi}}{\Psi^*_{mn}-(2\pi/T_{MN})}\right)\Bigg]\Bigg\}$$

$$+\sum_{m'=0}^{\mu}\sum_{n'=1}^{\nu}\mathrm{e}^{\mathrm{i}\psi^*_{m'n'}t}\left\{g^{(f)}_{m'n'}\left[\frac{F_0}{\mathrm{i}\psi^*_{m'n'}}\right.\right.$$

$$\left.-\frac{1}{2}\gamma\sum_{m=0}^{\mu}\sum_{n=1}^{\nu}\left(\frac{\Psi_{mn}w_{mn}}{\psi^*_{m'n'}+\Psi_{mn}}+\frac{\Psi^*_{mn}w^*_{mn}}{-\psi_{m'n'}+\Psi^*_{mn}}\right)\right]$$

$$+\frac{1}{2}\frac{\alpha}{T_{MN}}\frac{1}{\mathrm{i}}g^{(c)*}_{mn}\sum_{m=0}^{\mu}\sum_{n=1}^{\nu}\left[\frac{\Psi_{mn}w_{mn}(1-\mathrm{e}^{\mathrm{i}\Psi_{mn}T_{MN}})}{-\psi_{m'n'}-\Psi_{mn}}\right.$$

$$\times\left(-\frac{\mathrm{e}^{-\mathrm{i}\phi}}{\Psi_{mn}-(2\pi/T_{MN})}-\frac{\mathrm{e}^{\mathrm{i}\phi}}{\Psi_{mn}+(2\pi/T_{MN})}\right)$$

$$\left.\left.-\frac{\Psi^*_{mn}w^*_{mn}(1-\mathrm{e}^{-\mathrm{i}\Psi^*_{mn}T_{MN}})}{\mathrm{i}(-\psi^*_{m'n'}+\Psi^*_{mn})}\left(\frac{\mathrm{e}^{-\mathrm{i}\phi}}{\Psi^*_{mn}+(2\pi/T_{MN})}+\frac{\mathrm{e}^{\mathrm{i}\phi}}{\Psi^*_{mn}-(2\pi/T_{MN})}\right)\right]\right\}. \quad \text{(A10)}$$

This equation is satisfied if the constant terms as well as the coefficients of $\mathrm{e}^{-\mathrm{i}\Psi_{mn}t}$, $\mathrm{e}^{\mathrm{i}\Psi^*_{mn}t}$, $\mathrm{e}^{-\mathrm{i}\psi_{m'n'}t}$ and $\mathrm{e}^{\mathrm{i}\psi^*_{m'n'}t}$ are equal on either side of the equation.

Equating the coefficients of $\mathrm{e}^{-\mathrm{i}\Psi_{mn}t}$ gives

$$\Psi_{mn}\left[\frac{1}{2}\gamma\sum_{m'=0}^{\mu}\sum_{n'=1}^{\nu}\left(\frac{g^{(f)}_{m'n'}}{\Psi_{mn}-\psi_{m'n'}}+\frac{g^{(f)*}_{m'n'}}{\Psi_{mn}+\psi^*_{m'n'}}\right)\right.$$

$$+\frac{1}{2}\frac{\alpha}{T_{MN}}\mathrm{i}\,(1-\mathrm{e}^{-\mathrm{i}\Psi_{mn}T_{MN}})\left(\frac{\mathrm{e}^{-\mathrm{i}\phi}}{\Psi_{mn}-(2\pi/T_{MN})}+\frac{\mathrm{e}^{\mathrm{i}\phi}}{\Psi_{mn}+(2\pi/T_{MN})}\right)$$

$$\left.\times\sum_{m'=0}^{\mu}\sum_{n'=1}^{\nu}\left(\frac{g^{(c)}_{m'n'}}{\Psi_{mn}-\psi_{m'n'}}+\frac{g^{(c)*}_{m'n'}}{\Psi_{mn}+\psi^*_{m'n'}}\right)\right]=1,$$

$$(m=0,\ldots\mu,\ n=1,\ldots,\nu). \quad \text{(A11)}$$

This is a non-linear equation for the complex eigenfrequencies Ψ_{mn}; it also has roots $-\Psi^*_{mn}(m=0,\ldots\mu,\ n=1,\ldots,\nu)$. For the uncontrolled wheel ($\alpha=0$), it reduces to an equation which is equivalent to a polynomial equation of degree $2\mu\nu$. The equation is best solved numerically, for example with the Newton/Raphson method. A suitable starting value of the iteration would be $\Psi_{mn}=\psi_{mn}/(1-\frac{1}{2}\gamma g^{(f)}_{mn})$. This is the analytical estimate of the complex eigenfrequency of the uncontrolled friction-driven wheel (see equation (3.13) in reference [13]). It does not seem possible to derive from equation (A11) an equivalent analytical estimate

for the controlled case. The result (A11) is stated by equations (4.3) and (4.4) in the main text.

Equating the coefficients of $e^{i\Psi^*_{mn}t}$ in equation (A10) gives the complex conjugate of equation (A11). Equating the constants on either side of equation (A10) gives an explicit expression for real (w_0). Equating the coefficients of $e^{-i\psi_{m'n'}t}$ and $e^{i\psi^*_{m'n'}t}$ gives a linear set of equations for the complex amplitudes w_{mn} and w^*_{mn}.

A.2. RAIL VERSION OF THE ACTIVE CONTROL SYSTEM

The mathematical arguments for this version of the active control system are directly analogous to those described in the previous section. The governing equation (2.6) can be written with (A4) as

$$w(t) = \int_{t'=0}^{t} (F_f[v_w(r_f, \varphi_f, t') - v_r(t')]\, G(r_f, \varphi_f; r_f, \varphi_f; t - t'))\, dt'. \tag{A12}$$

Expression (A3) is substituted into the left-hand side of equation (A12). Substituted into the right-hand side of equation (A12) are the friction characteristic (4.5) and the Green's function (A2) evaluated at point (r_f, φ_f). Substituted into the argument of the friction characteristic are equation (A5) for the wheel velocity, and equation (2.7) for the rail velocity, where the control signal amplitude $A_{MN}(t')$ has been expressed by equation (A6). The resulting equation is

$$\begin{aligned}
&\frac{1}{2}\left[w_0 + w_0^* + \sum_{m=0}^{\mu}\sum_{n=1}^{\nu}(w_{mn}e^{-i\Psi_{mn}t} + w^*_{mn}e^{i\Psi^*_{mn}t})\right] \\
&\quad = \int_0^t \left[F_0 + \gamma\frac{1}{2}\sum_{m=0}^{\mu}\sum_{n=1}^{\nu}(-i\Psi_{mn}w_{mn}e^{-i\Psi_{mn}t'} + i\Psi^*_{mn}w^*_{mn}e^{i\Psi^*_{mn}t'})\right] \\
&\qquad \times\left[\frac{1}{2}\sum_{m'=0}^{\mu}\sum_{n'=1}^{\nu}(g^{(f)}_{m'n'}e^{-i\psi_{m'n'}(t-t')} + g^{(f)*}_{m'n'}e^{i\psi^*_{m'n'}(t-t')})\right]dt' \\
&\qquad + \int_0^t \frac{-\alpha\gamma}{T_{MN}}\frac{1}{2}\sum_{m=0}^{\mu}\sum_{n=1}^{\nu}\left[\Psi_{mn}w_{mn}\left(\frac{e^{-i\phi}}{\Psi_{mn} - (2\pi/T_{MN})} + \frac{e^{i\phi}}{\Psi_{mn} + (2\pi/T_{MN})}\right)\right. \\
&\qquad \times(1 - e^{i\Psi_{mn}T_{MN}})e^{-i\Psi_{mn}t'} \\
&\qquad \left. + \Psi^*_{mn}w^*_{mn}\left(\frac{e^{-i\phi}}{\Psi^*_{mn} + (2\pi/T_{MN})} + \frac{e^{i\phi}}{\Psi^*_{mn} - (2\pi/T_{MN})}\right)(1 - e^{-i\Psi^*_{mn}T_{MN}})e^{i\Psi^*_{mn}t'}\right] \\
&\qquad \times\left[\frac{1}{2}\sum_{m'=0}^{\mu}\sum_{n'=1}^{\nu}(g^{(f)}_{m'n'}e^{-i\psi_{m'n'}(t-t')}g^{(f)*}_{m'n'}e^{i\psi^*_{m'n'}(t-t')})\right]dt'.
\end{aligned} \tag{A13}$$

This result is very similar to its equivalent (A8) for the wheel version of the active control system; in fact, if the following replacements are made in equation (A8),

$$\alpha \to -\alpha\gamma \quad \text{and} \quad g^{(c)}_{m'n'} \to g^{(f)}_{m'n'}, \tag{A14a, b}$$

equation (A13) is obtained. It is therefore not necessary to derive the equation for the complex eigenfrequencies Ψ_{mn} by the lengthy manipulations outlined in the previous section. Instead, the equation can be constructed from equation (A11) by making the replacements (A14a, b). The result is

$$\Psi_{mn}\frac{1}{2}\gamma \sum_{m'=0}^{\mu}\sum_{n'=1}^{\nu}\left(\frac{g^{(f)}_{m'n'}}{\Psi_{mn}-\psi_{m'n'}}+\frac{g^{(f)*}_{m'n'}}{\Psi_{mn}+\psi_{m'n'}}\right)$$

$$\times\left[1-\frac{\alpha}{T_{MN}}\,\mathrm{i}(1-\mathrm{e}^{\mathrm{i}\Psi_{mn}T_{MN}})\left(\frac{\mathrm{e}^{-\mathrm{i}\phi}}{\Psi_{mn}-(2\pi/T_{MN})}+\frac{\mathrm{e}^{\mathrm{i}\phi}}{\Psi_{mn}+(2\pi/T_{MN})}\right)\right]=1$$

$$(m=0,\ldots\mu,\ n=1,\ldots,\nu). \tag{A15}$$

This result is stated by equation (4.6) with equation (4.4) in the main text.